A Novel Control Design for Realizing Passive Load-Holding Function on a Two-Motor-Two-Pump Motor-Controlled Hydraulic Cylinder

Wei Zhao [1]   Mohit Bhola [2]   Morten Kjeld Ebbesen [1]   Torben Ole Andersen [2]

[1] *Department of Engineering Sciences, University of Agder, N-4898 Grimstad, Norway. E-mail: wei.zhao@uia.no, morten.k.ebbesen@uia.no*

[2] *Mechatronics Section, Department of Energy Technology, Aalborg University, Aalborg, Denmark. E-mail: mobh@energy.aau.dk, toa@energy.aau.dk*

Abstract

When a hydraulic cylinder connects two chambers directly to one or two hydraulic pumps driven by electric servo motors without any control valve in between, it can be called a motor-controlled hydraulic cylinder (MCC). Unlike valve-controlled cylinders, MCCs have no valve throttling, which significantly increases the energy efficiency. Among different MCC topologies, the two-motor-two-pump (2M2P) MCC has several advantages, such as cylinder pressure control and no mode switch oscillations. However, due to state coupling when controlling both piston position and minimum cylinder chamber pressure, the 2M2P MCC is a multi-input-multi-output (MIMO) system that usually requires advanced MIMO controller analysis and design. This paper presents a control algorithm for a 2M2P MCC with the minimum cylinder pressure control and passive load-holding function. This control algorithm is tested on a single-boom crane characterized by overrunning loads. It is designed based on the analysis of the system characteristics, requiring no MIMO controller analysis and design. A non-linear model of a single-boom crane driven by the proposed 2M2P MCC is created in MATLAB/Simulink and experimentally validated. Feedback controllers are designed and verified via simulations to realize position control, minimum cylinder pressure control, and load-holding under standstill command. For a given load and speed profile, the hydraulic system efficiency during pumping and motoring mode is 55-60 % and 20-25 %, respectively. The system's overall efficiency can be enhanced with electrical regenerative drives, which feeds the generated power from potential energy to the grid or battery and reused in the next working cycle. The experimental results presented in this paper verifies the efficacy of the proposed control algorithm and demonstrates its superior performance in achieving the desired system response under various operating conditions.

Keywords: Motor-controlled hydraulic cylinder, pressure control, load-holding

1. Introduction

The hydraulic linear actuation system is extensively used in the industry for heavy load-carrying applications. Marine and offshore are major sectors that use a large number of hydraulic actuators in large-scale applications such as offshore cranes. The benefits of using hydraulic actuators in these applications are the high power-to-weight ratio, flexible power transmission, inherent damping quality, and high reliabil-

ity of the hydraulic systems. However, conventional valve-controlled hydraulic cylinders have long been associated with low energy efficiency, primarily due to the throttling effect caused by control valves Zimmerman et al. (2007). Given the rising global energy demand, environmental concerns, and the trend towards electrification and sustainable industrial practices, the need for efficient high-power hydraulic systems has become increasingly important. Such systems must be designed to deliver equivalent performance while minimizing energy consumption and promoting sustainable operation. Many researchers working on linear hydraulic systems are incorporating pump-controlled technology to enhance system efficiency. Quan et al. (2014) has done a literature review presenting pump-controlled cylinders of various topologies. The authors show the replacement of valve-controlled cylinders with none-valve cylinders, where the flow is varied by either the electric motor speed (motor-controlled hydraulic cylinders) or the pump displacement (pump-controlled cylinders). This is to remove the throttling losses in the system. Various shown topologies are suitable for particular applications. It also shows that motor-controlled cylinders (MCC) can generate energy using regenerative electrical drives. This enhances the efficiency of the system significantly. Figure 1 illustrates the general structure of MCCs. An MCC comprises two parts: a cylinder and a drive unit. The MCC drive unit contains electric motors, hydraulic pumps, accumulators, and auxiliary valves. In an MCC, the hydraulic cylinder is connected to one or two fixed-displacement hydraulic pumps and an oil reservoir through auxiliary valves. The auxiliary valves are used for the differential flow rates compensation and the load-holding capability. Electric servo motors drive the fixed-displacement hydraulic pumps.
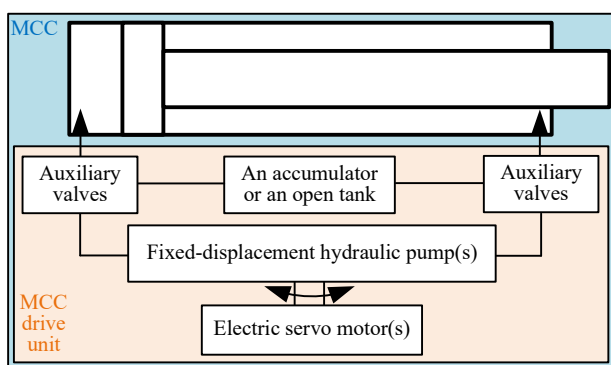
Figure 1: Structure of Motor-controlled cylinders

The work done by Fresia et al. (2022) shows the implementation of a novel layout on a hybrid excavator. The working hydraulics and boom actuation of the system is modified while achieving throttle-less motion and energy recovery in supercapacitors. According to the research, it saves around 26-28 % of fuel consumption as compared to conventional load-sensing functions. However, the research is going on the electro-mechanical actuators in parallel because of their higher efficiency but are commercially limited to lower power applications. This is due to its excessive mechanical wear and difficulty in overload protection Hagen et al. (2020). Hence, for higher load applications, MCCs seem to be a promising solution. The class of energy-efficient MCCs is discussed by Schmidt et al. (2019). It is concluded that with different hydraulic topologies and standard hydraulic components, MCCs can be scaled up to different applications. The energy-saving potential of these kinds of systems is estimated by Ketelsen et al. (2018) using simulations for a knuckle boom crane. It is observed that when carrying a load of 5 tons for a particular cyclic operation, a valve-controlled system consumes 0.79 kWh of electrical energy, whereas the proposed drive consumes 0.06 kWh. Another work done by Agostini et al. (2020) evaluates the energy efficiency of an MCC for a crane at a laboratory scale with energy regeneration capability. It is shown that the proposed system results in an efficiency of 54 % and 38 % with and without electrical energy regeneration, respectively. Additionally, another study Qu et al. (2020) demonstrated even higher efficiency, reaching up to 80 % in a laboratory application utilizing an MCC.

Despite the greater efficiency improvements offered by MCCs compared to conventional valve-controlled cylinders, the enforcement of load-holding capability by legislation poses challenges for MCCs. The application of counterbalance valves (CBVs) within an MCC is shown in Jalayeri et al. (2015) and Imam et al. (2017). This gives the passive load-holding capability of the system. However, it reduces the system's efficiency due to throttle losses occurring in the CBV. In addition to counterbalance valves, two on/off electric valves can be employed in MCCs to provide an active load-holding function without introducing throttling losses Zhang et al. (2017); Jensen et al. (2021). While normal-closed on/off electric valves can offer load-holding capabilities during power blackouts, achieving load-holding functions during hose ruptures or sudden drops in line pressure can present challenges. Another approach to achieve load holding is to utilize two pilot-operated check valves Parker (Accessed July 07, 2023); Sweeney T. (2012). However, using only two pilot-operated check valves without additional devices does not allow for four-quadrant operations, which are often required for large-size offshore knuckle boom cranes. To address this challenge, two pilot-

operated check valves and a solenoid valve as a load-holding device for cylinder locking are introduced by Hagen et al. (2018) and Padovani et al. (2019). The latter depresses the pilot line pressure during a power failure, preventing the load from falling. However, the operation of the system depends upon the condition of a solenoid valve, which only makes it partially passive. Also, the undesired oscillations are present during the opening/closing of the pilot-operated check valve. The solution to avoid these oscillations is developed by Hagen and Padovani (2020). The evaluation of a novel solution for a two-motor-two-pump (2M2P) MCC with fully passive load-holding capability is conducted in simulations by Ketelsen et al. (2020). Two 2/2 poppet-type pilot-operated valves are proposed as load-holding devices, each at the cylinder inlet and outlet. These valves are opened by the minimum cylinder pressure. An inverse shuttle valve (ISV) is used for always connecting the cylinder's minimum pressure for opening the load-holding valve. This 2M2P MCC is considered a multi-input-multi-output (MIMO) system, offering the flexibility to control both the minimum cylinder pressure and the cylinder's position by a specially designed MIMO controller. Yet, it is worth noting that designing the MIMO controller for such a system can be complex, requiring state coupling analysis and decoupler design. Furthermore, the MIMO controller needs to be tailored and designed specifically for each application to ensure optimal performance and functionality. From the above discussion, it can be concluded that only the 2M2P MCC has the possibility to offer a fully passive load-holding capability. However, it is important to note that the existing research on the 2M2P MCC is primarily limited to simulation studies. Additionally, the design and implementation of the MIMO controller for the 2M2P MCC is a highly intricate and customized process specific to each application. Therefore, further efforts are necessary to design a more universally applicable controller for 2M2P MCCs. Moreover, experimental studies are needed to validate the functionality of the 2M2P MCC and its practical viability.

In this paper, a novel control algorithm is designed and implemented on a 2M2P MCC with a passive load-holding capability on a laboratory-scale single-boom crane, which can be scaled up to various lifting applications. The energy efficiency of the proposed system is also evaluated experimentally. The open-loop simulation model of the 2M2P system is validated for future analysis. The paper is organized in the following sections. In Section 2, the hydraulic architecture and control algorithm of the system under investigation are presented. In Section 3, the experimental setup is discussed. In Section 4, the mathematical model of

the hydraulics and multi-body crane model in MATLAB/Simulink is made and validated for open-loop conditions. The experimental results obtained for the two-quadrant operation are described in Section 5 and discussed in Section 6. In Section 7, the outcome of the paper is concluded.

2. System under Investigation

In this paper, the novel solution named 2M2P MCC proposed by Ketelsen et al. (2020) is further explored with a novel control algorithm experimentally. The following subsections, System Architecture and Control Algorithm describe the system's topology and novel control algorithm with passive load-holding capability.

2.1. System Architecture
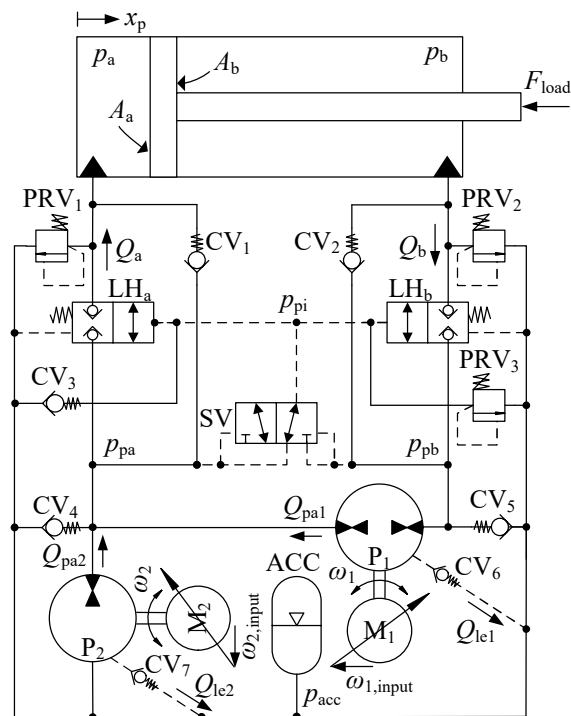
Figure 2: System architecture of the 2M2P MCC.

The 2M2P MCC under investigation comprises the two fixed-displacement pumps, the main pump (P_1) and the assisting pump (P_2), driven by two servo motors, the main electric servo motor (M_1) and the assisting electric motor (M_2), as illustrated in Figure 2. It is a closed-circuit system that can operate in four quadrants, along with the passive load-holding capability. The low-pressure accumulator (ACC) is used as the pressurized reservoir (3 bar) for supplying the volumetric difference (rod side and bore side of the cylinder) of
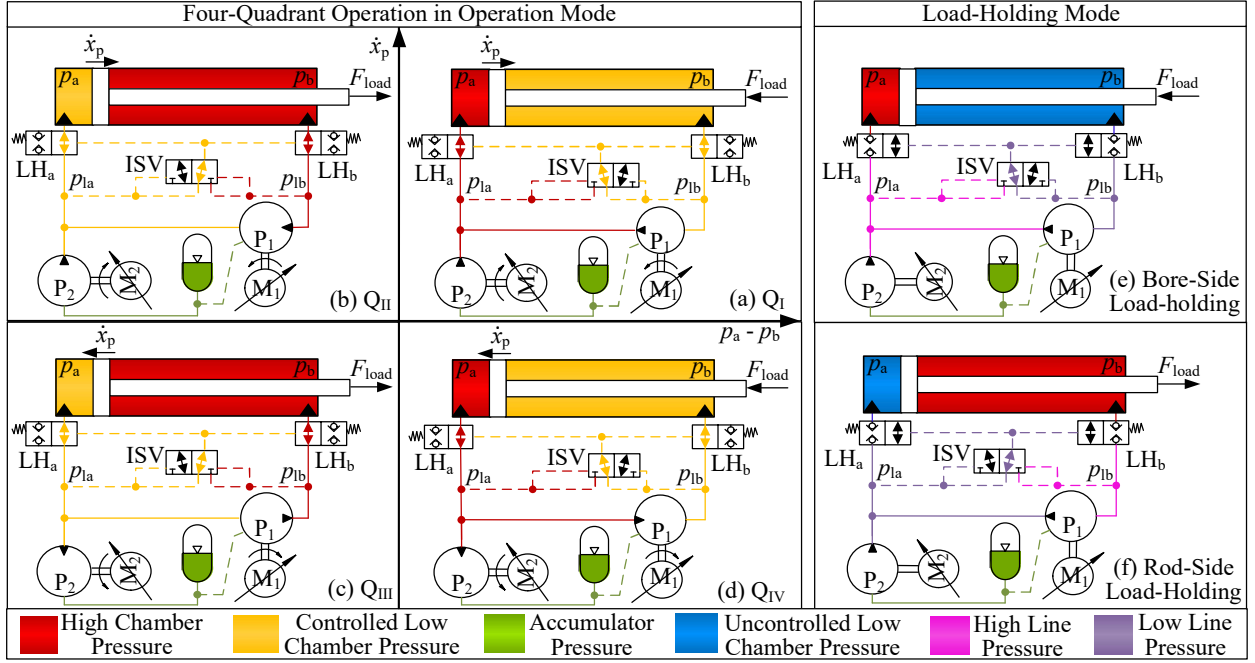
Figure 3: Demonstration of four-quadrant operation and load holding mode.

flow to the pumps during suction to avoid cavitation. The external leakage lines of pumps are connected with the low-pressure accumulator through two check valves (CV_6 and CV_7). The minimum cylinder pressure signal is used to open the 2/2 normally closed load holding valves (LH_a and LH_b). The opening functionality of load-holding valves is achieved by SV, a 3/2 hydraulic pilot-operated open-centered directional control valve. This valve changes its direction by the highest system pressure. It supplies the minimum cylinder pressure signal (p_{pi}) to open the load-holding valves. The load-holding valves are closed during the loss of pressure in pipelines. Two pressure relief valves (PRV_1 and PRV_2) are used to relieve the system's overpressure.

$$Q_{\mathbf{I}} = \begin{cases} \dot{x}_p > 0 \\ p_a > p_b \\ F_{load} < 0 \\ \omega_1 \cdot D_1 + \omega_2 \cdot D_2 = \dot{x}_p \cdot A_a \\ \omega_1 \cdot D_1 = \dot{x}_p \cdot A_b \end{cases} \quad (1)$$

The four-quadrant operation of the system is shown in Figure 3. P_1 functions as a pump in quadrants I and III, while P_2 serves as a pump in quadrant I and a motor in quadrant III. This is due to the excess oil that exits the bore side compared to the rod side for a given actuator speed. P_1 acts as a motor in quadrants II and IV, and P_2 acts as a pump in quadrant II and as a motor in quadrant IV. As in quadrant II, the extra amount of oil is to be pumped into the bore

side from ACC to control the minimum cylinder pressure. This is also explained mathematically with the following equations.

Referring to Equation 1, ω_1 and ω_2 are positive, this implies that both P_1 and P_2 operates as a pumps against positive pressure difference $p_a > p_b$ and $p_a > p_{acc}$. D_1 is the displacement of P_1. D_2 is the displacement of P_2. ω_1 is the shaft speed of M_1. ω_2 is the shaft speed of M_2. A_a and A_b are the bore-side and rod-side areas. $\dot{x}_p$ is the piston velocity. F_{load} is the external load force acting on the cylinder. When F_{load} is in the same direction as $\dot{x}_p$, it is an overrunning load. Otherwise, it is a resistant load.

$$Q_{\mathbf{II}} = \begin{cases} \dot{x}_p > 0 \\ p_a < p_b \\ F_{load} > 0 \\ \omega_1 \cdot D_1 + \omega_2 \cdot D_2 = \dot{x}_p \cdot A_a \\ \omega_1 \cdot D_1 = \dot{x}_p \cdot A_b \end{cases} \quad (2)$$

Referring to Equation 2, ω_1 and ω_2 are positive, this implies that the rotation of P_1 and P_2 are similar as quadrant I. P_1 operates under negative pressure difference $p_a < p_b$, thus acts as a motor, and P_2 operates under positive pressure difference $p_a > p_b$, thus acts as a pump.

$$Q_{\mathbf{III}} = \begin{cases} \dot{x}_p < 0 \\ p_a < p_b \\ F_{load} > 0 \\ \omega_1 \cdot D_1 + \omega_2 \cdot D_2 = \dot{x}_p \cdot A_a \\ \omega_1 \cdot D_1 = \dot{x}_p \cdot A_b \end{cases} \quad (3)$$

Referring to Equation 3, ω_1 and ω_2 are negative, this implies that the rotation of P_1 and P_2 are opposite as quadrant I. Also, the rod-side pressure is higher than the bore-side pressure. The P_2 works as a motor as it operates in negative pressure difference $p_a < p_{acc}$. However, P_1 works against the positive pressure difference $p_b > p_a$ and operates as a pump.

$$Q_{\mathbf{IV}} = \begin{cases} \dot{x}_p < 0 \\ p_a > p_b \\ F_{load} < 0 \\ \omega_1 \cdot D_1 + \omega_2 \cdot D_2 = \dot{x}_p \cdot A_a \\ \omega_1 \cdot D_1 = \dot{x}_p \cdot A_b \end{cases} \tag{4}$$

Referring to Equation 4, ω_1 and ω_2 are negative and $p_a > p_b$. Therefore, P_1 and P_2 act as motors as they work against the negative pressure difference.

2.2. Control Algorithm

The 2M2P MCC under investigation is a MIMO system, where inputs $\omega_{1,input}$ and $\omega_{2,input}$ of M_1 and M_2 are the system inputs, and piston position x_p and the minimum cylinder pressure p_{pa} or p_{pb} are the required system outputs. A control algorithm is developed based upon the steady-state analysis of the system in four quadrants as explained in Section 2.1. The control algorithm designed for the proposed 2M2P MCC is demonstrated in Figure 4. The switching logic of the mode and inputs selection module is shown in Figure 5. This control algorithm consists of four control loops for a smooth transition between motion and load-holding modes. These four loops are the position control loop, cylinder pressure control loop, load-holding control loop, and pressure level control loop. Each control loop generates two reference speeds $\omega_{1,ref}$ and $\omega_{2,ref}$ for M_1 and M_2. These speed references are fed into the mode and inputs selection algorithm to generate the final speed inputs to M_1 and M_2 according to four-quadrant operations. There are two working modes: motion mode and load-holding mode. When the cylinder speed reference $\dot{x}_{ref}$ is zero, the system is in load-holding mode. Otherwise, the system is in motion mode. Four control loops are described in the following subsections.

2.2.1. Position Control Loop

The green area in Figure 4 shows the position control loop. The position control loop is activated in motion mode. A feedforward controller estimates the required speed of M_1 (u_{ff}) via Equation 5.

$$u_{ff} = \frac{\dot{x}_{ref} \cdot A_b}{D_1} \tag{5}$$

The position controller, a proportional-integral controller, corrects the prediction of the feedforward controller. The proportional gain (k_P) is 70 rev/min/m and the integral gain (k_I) is 15 rev/min/m/s.

A load-pressure feedback signal (p_L) calculated via the bore-side pressure (p_a), the rod-side pressure (p_b), and the

area ratio (A_b/A_a) is filtered by a high-pass filter (G_{HP}) shown in Equation 6. The filter cut-off frequency (ω_{HP}) is 10 rad/s. The filter gain (k_{HP}) is 20 rev/min/bar. The negative filtered load-pressure feedback signal is added to increase the system damping by canceling out pressure oscillations.

$$G_{HP} = k_{HP} \cdot \frac{s}{s + \omega_{HP}} \tag{6}$$

In the proposed 2M2P MCC, the main hydraulic pump (P_1) moves hydraulic oil in the annular volume from one side to the other side of the cylinder. When the piston moves, the assist pump (P_2) compensates for the cylinder differential volume, which is also the rod volume. When two pumps' flow rates match the cylinder area ratio, the system works smoothly without cavitation or overpressure. Therefore, the total position control loop output (u_{pos}) is multiplied by a speed gain to make the two pumps' flow rates match the cylinder area ratio. For the system under investigation, the pump displacement ratio (D_1/D_2) is 2.0 and the area ratio of rod area over annulus area (A_r/A_b) is 1.04, hence the speed gain (k_{speed}) is 2.08.

2.2.2. Cylinder Pressure Control Loop

The purple area in Figure 4 shows the cylinder pressure control loop. The cylinder pressure control loop is activated in motion mode. As described in Section 2.1, the minimum cylinder pressure needs to be over 10 bar to activate the load-holding valves in motion mode and to be less than 10 bar to deactivate the load-holding valves in load-holding mode. The minimum pressure between p_{pa} and p_{pb} is chosen as the feedback signal through the minimum cylinder pressure selection algorithm. The cylinder pressure reference signal in the loop is set to 25 bar. The cylinder pressure controller is a proportional-integral controller. The proportional gain (k_P) is 20 rev/min/bar, and the integral gain (k_I) is 5 rev/min/bar/s. The controller outputs are applied on M_1 ($\omega_{1,ref}$) in quadrants I and IV and on M_2 ($\omega_{2,ref}$) in quadrants II and III, via the mode and inputs selection block.

2.2.3. Load-Holding Control Loop

The orange area in Figure 4 shows the load-holding control loop. This control loop is activated in load-holding mode. As shown in Figure 3, two scenarios exist when the 2M2P MCC turns from motion mode to load-holding mode. In one scenario, the 2M2P MCC turns from quadrants I and IV to piston-side load-holding mode shown in Figure 3(e). In this case, pressure p_{pa} carries the load, and pressure p_{pb} controls the load-holding valves. Therefore, the load-holding pressure controller needs to decrease the pressure p_{pb} to deactivate the load-holding valves without affecting the pressure p_{pa}, which is holding the piston position. This is done by adding the negative controller output signal on the main and assist servo motors, where the signal on the assist servo motor needs to be doubled because the pump displacement ratio (D_1/D_2) is 2.0. In this way, the oil in the chamber forming pressure p_{pb} is pumped by P_1 and P_2 to the accumulator, while the oil in the chamber forming
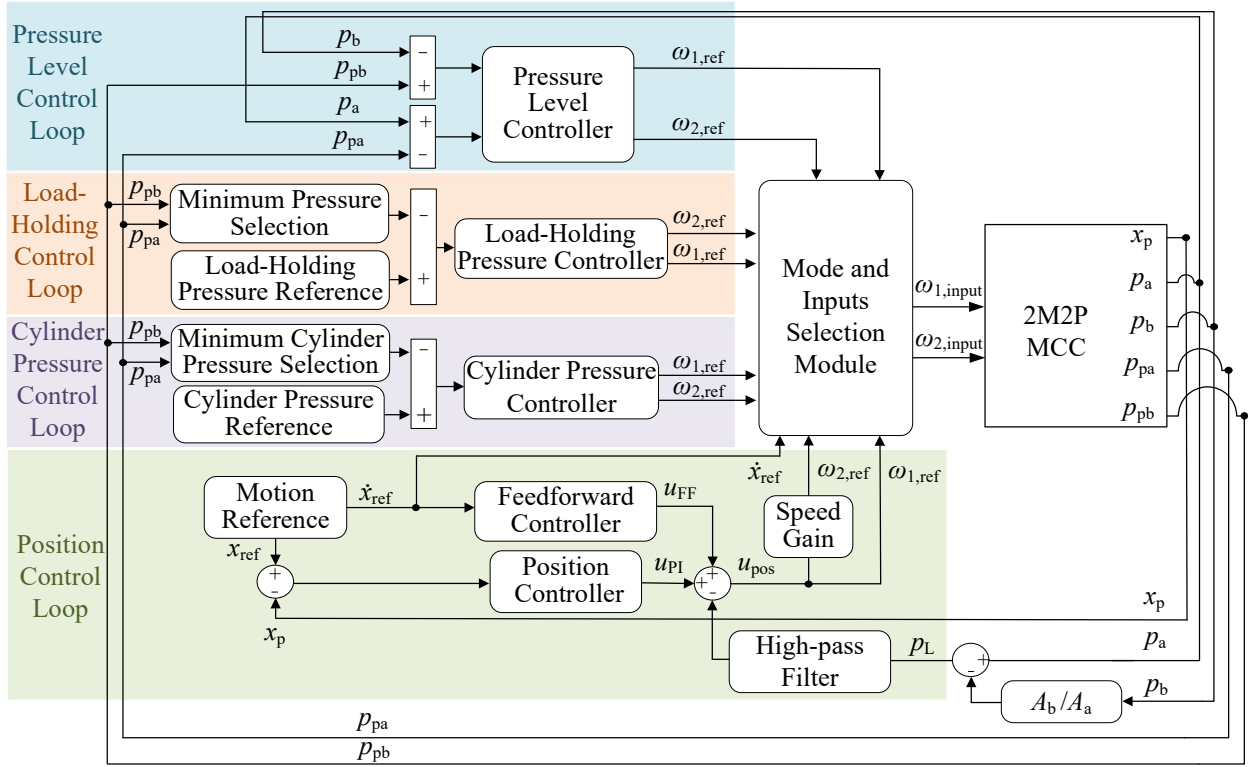
Figure 4: Realization of the control algorithm.

pressure p_{pa} stays the same. Therefore, the cylinder position is maintained during the transient period.
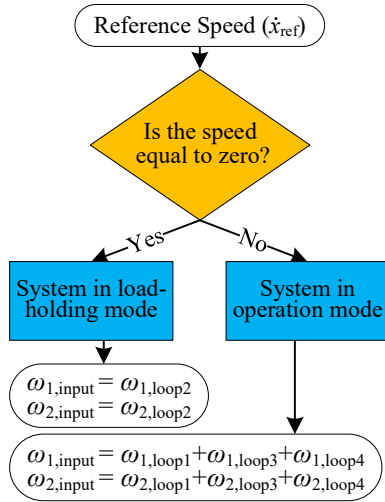
Figure 5: Switching logic of the mode and inputs selection module.

In the other scenario, the 2M2P MCC turns from quadrants II and III to rod-side load-holding mode shown in Figure 3(f). In this case, pressure p_{pb} carries the load, and pressure p_{pa} controls the load-holding valves. The load-holding pressure controller only needs to be applied on M$_2$

while M$_1$ stands still. Therefore, pressure p_{pa} is reduced by the controller to deactivate the load-holding valves and pressure p_{pb} stays the same to hold the cylinder position during the transient period. The load-holding pressure controller is a proportional-integral controller. The proportional gain (k_P) is 25 rev/min/bar, and the integral gain (k_I) is 3 rev/min/bar/s.

2.2.4. Pressure Level Control Loop

The blue area in Figure 4 shows the pressure level control loop. This control loop is activated during the transition from load-holding mode to motion mode. There are two reasons for designing this control loop. One reason is that pressures on two sides of the load-carrying side load-holding valve, p_a and p_{pa} in quadrants I and IV or p_b and p_{pb} in quadrants II and III, should be the same when the load-holding valves are activated. In this case, the piston position is maintained during the transient period from load-holding to motion mode.

The other reason is that when the system is in transition from load-holding mode to motion mode, the SV oscillates severely if the magnitude of p_{pa} is similar to the magnitude of p_{pb}. Therefore, the controller needs to quickly increase the pressure before the load-carrying side load-holding valve (p_{pa} in quadrants I and IV or p_{pb} in quadrants II and III) to the load pressure (p_a in quadrants I and IV or p_b in quadrants II and III) to prevent oscillations of SV.

The pressure level controller is a proportional-integral controller. The proportional gain (k_P) is 92 rev/min/bar,

and the integral gain (k_I) is 4 rev/min/bar/s. The controller output is applied to M_2 during the system's transition from the piston-side load-holding mode (shown in Figure 3(e)) to the motion modes in quadrants I and IV (shown in Figures 3(a) and 3(d), respectively). In contrast, the controller output is applied to M_1 during the system's transition from the rod-side load-holding mode (shown in Figure 3(f)) to the motion modes in quadrants II and III (shown in Figures 3(b) and 3(c), respectively).

3. Experimental Setup

The experiments are performed on a single-boom crane driven by the proposed 2M2P MCC located at Aalborg University, Denmark. The 2M2P MCC drive unit, the single-boom crane, and the control cabinet are presented in Figure 6. The single-boom crane has the capability to operate in quadrants I and IV, i.e., it provides resisting and assisting loads during cylinder extending and retracting motions, respectively. This experimental testbench also gives the possibility to validate the passive load-holding functionality of the system. The testing of the 2M2P MCC on the single-boom crane is challenging and interesting to validate due to its inherited enhanced oscillations because of its design.

The 2M2P test bench comprises the two electric servo motors, M_1 and M_2, which drive the two fixed-displacement axial piston pumps, P_1 and P_2. The flow rate from the pumps is adjusted by varying rotational speeds of M_1 and M_2. The rotational speeds of M_1 and M_2 are changed by the dedicated electrical drives, which get speed commands from the programmable logic controller (PLC) provided by Bosch Rexroth. The 3/2 hydraulic pilot-operated SV is deployed in the circuit to provide the pilot pressure (p_{pi}) to normally closed load-holding valves (LH_a and LH_b). The load-holding valves are the spring return (set at 10 bar) logic elements that isolate the fluid supply to the cylinder during the pressure loss from the pump. In real crane applications, the load-holding valves have to be installed as an integral part of the cylinder inlet and outlet to prevent the crane from falling during hose rupture conditions.

The two check valves (cracking pressure 0.2 bar), CV_1 and CV_2, are installed parallel to the LH valves to improve the system response. The hydraulic accumulator, sized according to the cylinder area ratio and length, is installed to provide the differential flow to the cylinder and avoid cavitation. The cross port pressure relief valves (Maximum set pressure 240 bar) are also installed in the circuit to avoid over-pressurization. To make the system compact, all the valves deployed are of cavity design which is kept inside the manifold.

The sensors used are draw-wire sensors for monitoring the piston position, and pressure sensors of different ranges are used for monitoring the pressure in the lines. The speed and position of M_1 and M_2 are monitored through inbuilt standard encoders. For executing the control algorithms, the PLC (XM22) with digital and analog I/O's extensions by Bosch Rexroth with SERCOS communication is used. The data acquisition from the sensors and programming of PLC are made on Indraworks Engineering software. The technical specifications of the major components used in the system are described in Table 1 in Appendix B.

4. System Modelling and Validation

Multiple dynamic models of the 2M2P MCC driving the single-boom crane were created and simulated in MATLAB-Simulink®.

4.1. 3D Crane Model

A multibody 3D model of the single-boom crane with rigid body components is constructed in the Simulink-Simscape environment by importing the crane CAD model. In this model, a cylindrical joint works as a hydraulic cylinder. The actuation force to the cylindrical joint is from the 2M2P MCC model. The position and velocity measurements of the cylindrical joint are fed back to the 2M2P MCC model. This rigid 3D multibody crane model and the connection to the 2M2P MCC model are shown and further discussed in Appendix A.

4.2. Dynamic Modeling of the 2M2P MCC

4.2.1. Electric Servo Motor

Two electric servo motors (M_1 and M_2) are modeled by second-order transfer functions shown in Equation 7 and 8. These transfer functions are from M_1 and M_2 input signals ($\omega_{1,ref}$ and $\omega_{2,ref}$) to hydraulic pump shaft speeds (ω_1 and ω_2). The natural frequencies and the damping ratios are determined using the embedded parameter estimator toolbox in Simulink against experimental data. The natural frequencies are $\omega_{em1} = 23.8$ Hz and $\omega_{em2} = 12.6$ Hz. The damping ratios are $\zeta_{em1} = 0.73$ and $\zeta_{em2} = 0.79$.

$$G_{M1}(s) = \frac{\omega_{M1}^2}{s^2 + 2 \cdot \omega_{M1} \cdot \zeta_{M1} \cdot s + \omega_{M1}^2} \tag{7}$$

$$G_{M2}(s) = \frac{\omega_{M2}^2}{s^2 + 2 \cdot \omega_{M2} \cdot \zeta_{M2} \cdot s + \omega_{M2}^2} \tag{8}$$

4.2.2. Fixed-Displacement Hydraulic Pumps

Two fixed-displacement hydraulic pumps (P_1 and P_2) are the hydraulic power source in the circuit. Because they are rigidly connected to the electric motor, they have the same angular speeds (ω_1 and ω_2) as the electric servo motors. The pump's dynamics is combined with the electric motor's dynamics and represented via Equation 7 and 8. The pump flow rates (Q_{pa1} and Q_{pa2}) are modeled via Equation 9 and 10. $D_1 = 6$ cc/rev and $D_2 = 3$ cc/rev are hydraulic pump displacements.

$$Q_{pa1} = D_1 \cdot \omega_1 \tag{9}$$

$$Q_{pa2} = D_2 \cdot \omega_2 \tag{10}$$

The leakages ($Q_{le,high}$ and $Q_{le,low}$) in P_1 are modeled via Equations 11 and 12. Δp_h is the pressure difference between the pump high-pressure side and the accumulator. Δp_l is the pressure difference between the pump low-pressure side and the accumulator.
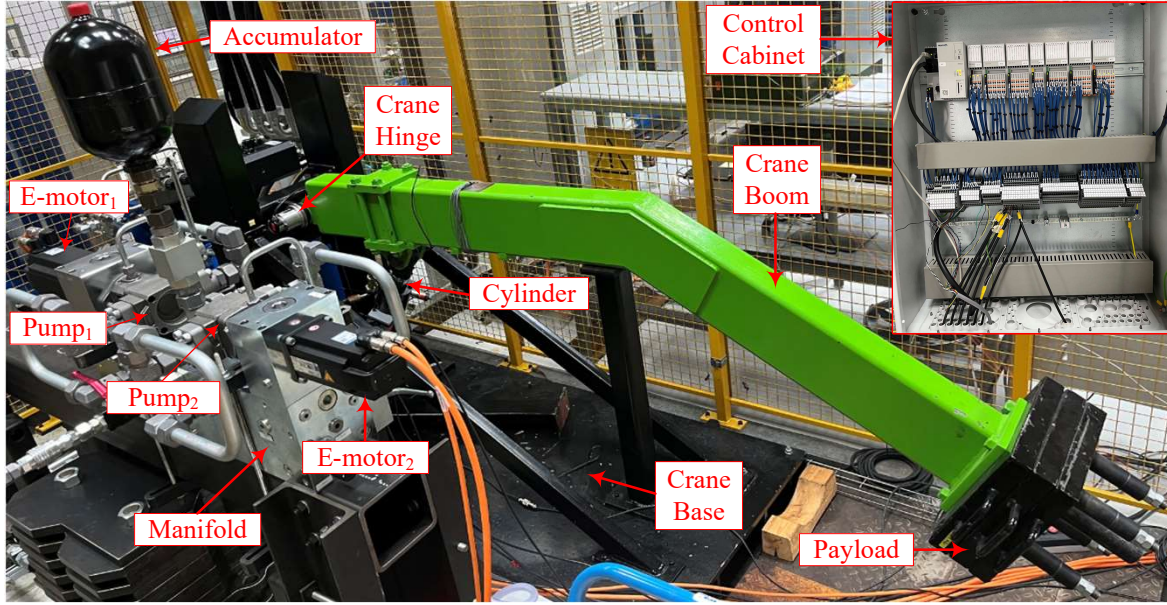
Figure 6: Experimental testbench including 2M2P MCC drive unit, single-boom crane, and control cabinet.

$k_{le1} = 2.5 \cdot 10^{-3}$ L/min/bar is the main hydraulic pump leakage coefficient. The total leakage of the main hydraulic pump is modeled via Equation 12.

$$Q_{le,high} = \Delta p_h \cdot k_{le1} \qquad (11)$$

$$Q_{le,low} = \Delta p_l \cdot k_{le1} \qquad (12)$$

$$Q_{le1} = Q_{le,high} + Q_{le,low} \qquad (13)$$

Because the P_2 low-pressure side is connected to the accumulator, the leakage ($Q_{le,assist}$) in P_2 is modeled via Equation 14. Δp_{assist} is the pressure difference between two sides of the assist hydraulic pump. $k_{le2} = 5.6 \cdot 10^{-3}$ L/min/bar is the assist hydraulic pump leakage coefficient.

$$Q_{le2} = \Delta p_{assist} \cdot k_{le2} \qquad (14)$$

4.2.3. Effective Bulk Modulus

The hydraulics is modeled utilizing a consolidated approach. The effective fluid's bulk modulus ($\beta_{chb,i}$) in the i-th hydraulic chamber is calculated via Equations 15, 16, and 17. $\beta_{oil} = 7000$ bar is the hydraulic oil's bulk modulus. $p_{chb,i}$ is the pressure in i-th hydraulic chamber. $p_{atm} = 1$ bar is the atmospheric pressure. $k_{air} = 1.4$ is the air adiabatic constant. $\beta_{chb,air,i}$ is the i-th chamber entrapped air bulk modulus. $V_{atm,\%air} = 0.01$ is the entrapped air relative volume when the oil is in the open air. $V_{chb,\%air,i}$ is the entrapped air relative volume in i-th chamber oil.

$$\beta_{chb,air,i} = p_{chb,i} \cdot k_{air} \qquad (15)$$

$$V_{chb,\%air,i} = V_{atm,\%air} \cdot \left(\frac{p_{atm}}{p_{chb,i}} \right)^{\frac{1}{k_{air}}} \qquad (16)$$

$$\beta_{chb,i} = \frac{1}{\frac{1}{\beta_{oil}} + \frac{V_{chb,\%air,i}}{\beta_{chb,air,i}}} \qquad (17)$$

4.2.4. Hydraulic cylinder

A hydraulic cylinder model comprises four parts: pressure build-up, pressure-force conversion, stroke limits, and cylinder friction. Pressure build-ups on the bore side ($\dot{p}_a$) and rod side ($\dot{p}_b$) of the cylinder are modeled via Equations 18 and 19. Q_a and Q_b are the flow rates going in or out of the cylinder bore and rod sides. x_p and $\dot{x}_p$ are the piston position and velocity, respectively. A_a and A_b are the bore and rod side areas. $x_{end} = 400$ mm is the cylinder stroke end. V_0 is the cylinder dead volume plus line volume.

$$\dot{p}_a = \frac{\beta_{chb,a} \cdot (Q_a - \dot{x}_p \cdot A_a)}{V_0 + x_p \cdot A_a} \qquad (18)$$

$$\dot{p}_b = \frac{\beta_{chb,b} \cdot (\dot{x}_p \cdot A_b - Q_b)}{V_0 + (x_{end} - x_p) \cdot A_b} \qquad (19)$$

The pressure-force conversion (F_{cyl}) is modeled via Equation 20.

$$F_{cyl} = p_a \cdot A_a - p_b \cdot A_b \qquad (20)$$

The cylinder stroke limit contact forces (F_{lower} and F_{upper}) are modeled via Equations 21 and 22. $k_c = 6 \cdot 10^{10}$ N/m is the contact spring constant. $c_c = 9 \cdot 10^{10}$ Ns/m is the contact damping coefficient.

$$F_{lower} = \begin{cases} 0 & x_p \geq 0 \\ x_p \cdot k_c + \dot{x}_p \cdot c_c & x_p < 0 \end{cases} \qquad (21)$$

$$F_{upper} = \begin{cases} 0 & x_p \leq x_{end} \\ (x_p - x_{end}) \cdot k_c + \dot{x}_p \cdot c_c & x_p > x_{end} \end{cases} \qquad (22)$$

The friction between cylinder and piston is modeled via the Stribeck curve Equation 23. $f_v = 4000$ Ns/m is the viscous friction coefficient. $F_C = 75$ N is the coulomb friction force. $\gamma = 250$ s/m is the hyperbolic tangent coefficient.

$F_S = 500$ N is the static friction force. $\tau = 0.02$ s/m is the static friction time constant.

$$F_f = f_v \cdot \dot{x}_p + \tanh(\gamma \cdot \dot{x}_p) \cdot \left(F_C + F_S \cdot e^{\frac{-\dot{x}_p \cdot \tanh(\gamma \cdot \dot{x}_p)}{\tau}} \right) \quad (23)$$

4.2.5. Accumulator

The bladder accumulator is modeled using the method suggested in Hansen (2023). As shown in Equation 24, the gas pressure (p_g) is equal to the fluid pressure (p_f) when the fluid pressure is higher than the pre-charge gas pressure $(p_{g0} = 0.96$ bar).

$$p_g = p_f(p_f \geq p_{g0}) + p_{g0}(p_f < p_{g0}) \quad (24)$$

When the gas pressure changes, the gas volume (V_g) is modeled via Eq. 25. $n = 1.4$ is the ratio of the gas heat.

$$V_g = \left(\frac{p_{g0} \cdot V_{g0}^n}{p_g} \right)^{\frac{1}{n}} \quad (25)$$

The fluid volume (V_f) is calculated as the difference in total accumulator volume $(V_{g0} = 2.8$ L) and gas volume (V_g):

$$V_f = V_{g0} - V_g \quad (26)$$

The fluid pressure build-up $(\dot{p}_f)$ is modeled via Eq. 27.

$$\dot{p}_f = \frac{\beta_{chb,acc}}{V_f} \cdot (Q_{acc} - \dot{V}_f) \quad (27)$$

The accumulator pressure (p_{acc}) is equal to the fluid pressure (p_f).

4.2.6. Pressure Relief Valves (PRV)

The bore and rod side PRVs are modeled via Equation 28 to 31. Q_{prv1} and Q_{prv2} are the flow rates passing through two PRVs. $k_{prv} = 500$ L/min/bar is the PRV flow rate constant. $p_{prv1} = p_{prv2} = 250$ bar are the PRV cracking pressures.

$$\Delta p_a = p_a - p_{acc} \quad (28)$$

$$Q_{prv1} = \begin{cases} 0 & (\Delta p_a - p_{prv1}) \leq 0 \\ (\Delta p_a - p_{prv1}) \cdot k_{prv} & (\Delta p_a - p_{prv1}) > 0 \end{cases} \quad (29)$$

$$\Delta p_b = p_b - p_{acc} \quad (30)$$

$$Q_{prv2} = \begin{cases} 0 & (\Delta p_b - p_{prv2}) \leq 0 \\ (\Delta p_b - p_{prv2}) \cdot k_{prv} & (\Delta p_b - p_{prv2}) > 0 \end{cases} \quad (31)$$

PRV$_3$ is on the pilot pressure line (p_{pi}). The flow rate passing through PRV3 is modeled via Equation 33. The cracking pressure (p_{prv3}) is set to 100 bar.

$$\Delta p_{pi} = p_{pi} - p_{acc} \quad (32)$$

$$Q_{prv3} = \begin{cases} 0 & (\Delta p_{pi} - p_{prv3}) \leq 0 \\ (\Delta p_{pi} - p_{prv3}) \cdot k_{prv} & (\Delta p_{pi} - p_{prv3}) > 0 \end{cases} \quad (33)$$

4.2.7. Check Valves (CV)

As shown in Figure 2, there are seven CVs in the 2M2P MCC. They are all modeled via Equation 34. $Q_{cv,i}$ is the flow rate passing through the i-th CV. $\Delta p_{cv,i}$ is the pressure drop across the i-th CV. The cracking pressure $p_{cv} = 0.2$ bar is the same for all CVs. The CV flow rate constant $k_{cv} = 500$ L/min/bar is also the same for all CVs.

$$Q_{cv,i} = \begin{cases} 0 & (\Delta p_{cv,i} - p_{cv}) \leq 0 \\ (\Delta p_{cv,i} - p_{cv}) \cdot k_{cv} & (\Delta p_{cv,i} - p_{cv}) > 0 \end{cases} \quad (34)$$

4.2.8. Inverse Shuttle Valve (ISV) and Load-Holding Valves (LH)

The ISV is modeled as a single selection logic shown in Equation 35. p_{pa} is the pressure between LH$_a$ and the assist hydraulic pump (P$_2$). p_{pb} is the pressure between LH$_b$ and the main hydraulic pump (P$_1$).

$$p_{pi} = \begin{cases} p_{pa} & p_{pa} \leq p_{pb} \\ p_{pb} & p_{pa} > p_{pb} \end{cases} \quad (35)$$

The LH$_a$ and LH$_b$ are modeled as orifices. Flow rates $(Q_{lha}$ and $Q_{lhb})$ passing through LH$_a$ and LH$_b$ are calculated via Equations 36 and 37. $C_d = 0.7$ is the orifice discharge coefficient. u_{lha} and u_{lhb} are valve opening commands. $A_{lha} = A_{lhb} = 200$ mm^2 are valve maximum opening areas. $\rho = 870$ kg/m^3 is the hydraulic oil density.

$$Q_{lha} = C_d \cdot u_{lha} \cdot A_{lha} \cdot \sqrt{\frac{2 \cdot |p_a - p_{pa}|}{\rho}} \cdot \text{sign}(p_a - p_{pa}) \quad (36)$$

$$Q_{lhb} = C_d \cdot u_{lhb} \cdot A_{lhb} \cdot \sqrt{\frac{2 \cdot |p_b - p_{pb}|}{\rho}} \cdot \text{sign}(p_b - p_{pb}) \quad (37)$$

u_{lha} and u_{lhb} are provided by the logic:

$$u_{lha} = u_{lhb} = \begin{cases} 1 & p_{pi} > p_{lh} \\ 0 & p_{pi} \leq p_{lh} \end{cases} \quad (38)$$

$p_{lh} = 10$ bar is the load-holding cracking pressure.

4.3. Open-Loop Model Validation

The nonlinear dynamic model of the 2M2P MCC was validated against experimental measurements. The open-loop speed input commands for the main and assist electric servo motors, as shown in Figure 7, drive the cylinder to extend and retract. Figures 8 to 13 show good agreements between measured and simulated variables, confirming the high-fidelity nature of the dynamic model. Therefore, it is a good simulation tool for further control analyses.
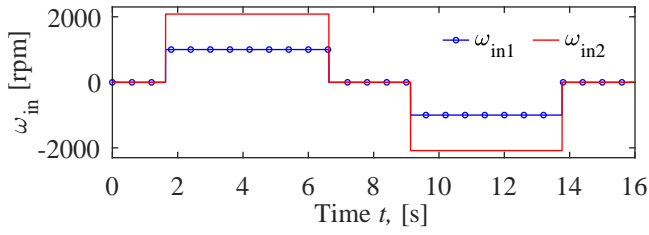
Figure 7: Electric servo motor input signals.
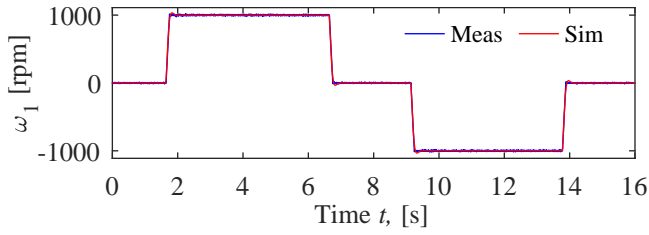
Figure 8: Main servo motor speeds.
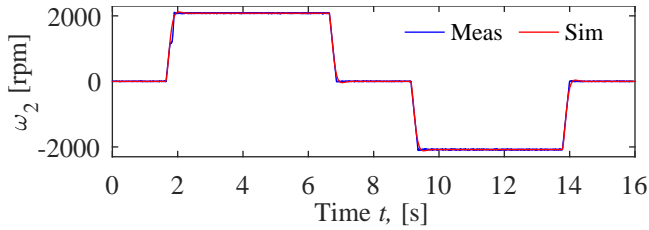
Figure 9: Assisting servo motor speeds.
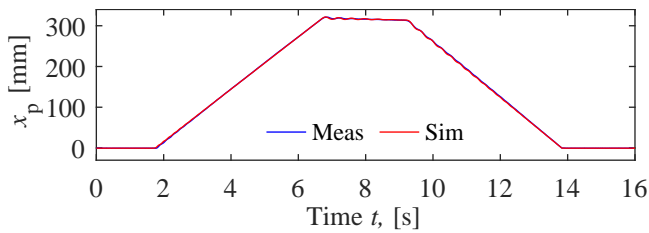
Figure 10: Piston positions.
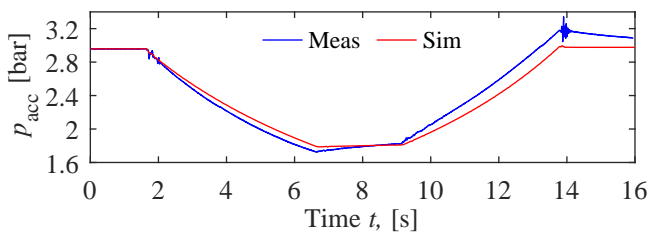
Figure 11: Accumulator pressure.
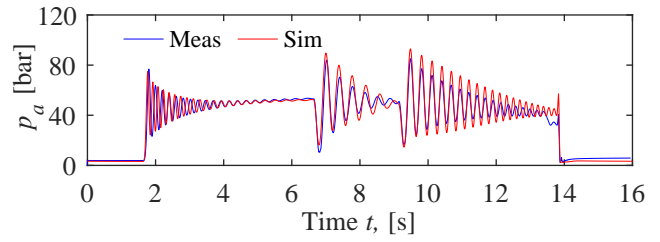
Figure 12: Bore-side pressure.
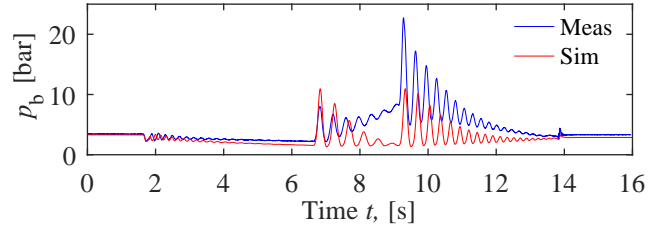
Figure 13: Rod-side pressure.

5. Experimental Results

A representative working trajectory consisting of extending and retracting the hydraulic cylinder across three load-holding operating sections is used as the piston position command. This command corresponds to a piston velocity of 20 mm/s, which is the typical working speed for this type of crane. By analyzing system performance when controlled by the algorithm shown in Figure 4, the chosen trajectory allows for an assessment of the algorithm's effectiveness. The experimental results are presented and analyzed in subsequent subsections. Note that LH in the following plots represents the load-holding mode, while pumping and motoring refer to pumping and motoring modes, respectively.

5.1. Position Tracking Performance

The commanded and measured piston position and the position tracking error are presented in Figure 14a and 14b. The measured position follows the commanded position well. The tracking error falls within -3.2 mm to 2.3 mm. The error peaks at points A, B, and C, appear when the system turns from load-holding to motion mode. The average error of the whole period is 0.39 mm. The position tracking performance is satisfactory since the maximum position error of hydraulic cranes is not uncommon to be bigger than 15 mm Kjelland and Hansen (2015).

5.2. Minimum Cylinder Pressure Control Performance

The proposed 2M2P MCC offers the advantage of cylinder pressure control, a capability not present in the 1M1P MCC Padovani et al. (2019). The minimum pressure between p_{pa} and p_{pb} is controlled to activate or deactivate LH

(a) Commanded and measured piston positions.

(b) Piston position error.
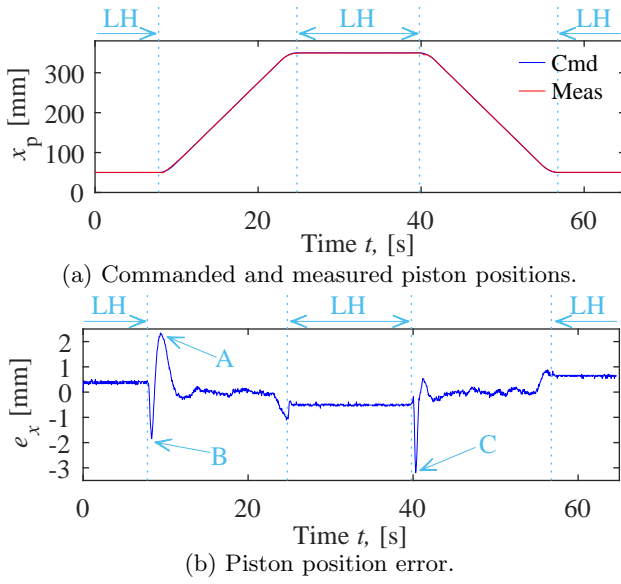
Figure 14: Position tracking performance.

valves. The minimum cylinder pressure control reference is 25 bar. Because the hydraulic cylinder drives the crane only in quadrants I and IV, p_{pb} is always the minimum or the controlled cylinder pressure. Measured pressures p_a and p_{pa} are shown in Figure 15. Measured pressures p_b and p_{pb}
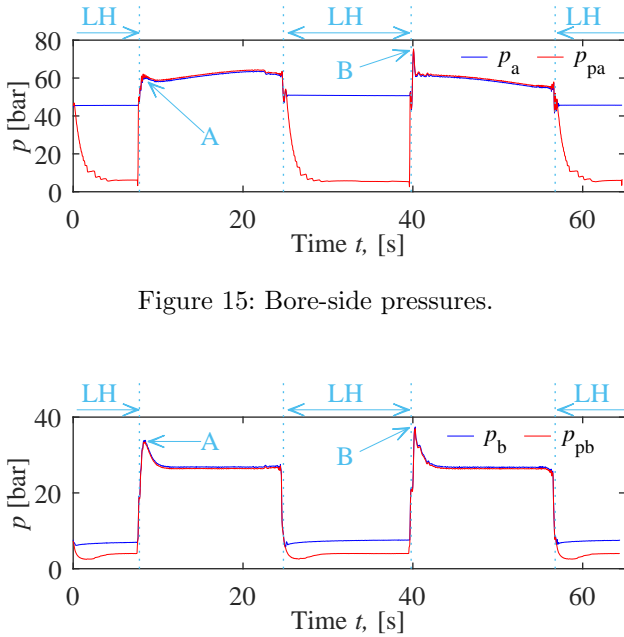
Figure 15: Bore-side pressures.

Figure 16: Rod-side pressures.

are shown in Figure 16. In motion mode, p_{pa} and p_{pb} are almost equal to p_a and p_a. In load-holding mode, because of the activated load-holding valves, p_a stays at a certain pressure level to hold the load while p_{pa} drops to approximately 5 bar due to the internal leakages across the two hydraulic pumps. Because p_{pb} is the minimum pressure activating

and deactivating load-holding valves, it is controlled in both motion and load-holding modes. In motion mode, p_{pb} is settled at approximately 26 bar after a short period, where the control reference is 25 bar. In load-holding mode, after a short period, p_{pb} is settled at approximately 4 bar, the same as the control reference. System pressures show stable behavior and smooth transitions between load-holding and motion modes, except for two pressure peaks at points A and B in the figures. Furthermore, it is noteworthy to highlight the stability and smoothness of system pressure behavior exhibited in MCC. This stands in contrast to hydraulic cranes equipped with standard load-holding valves, which may encounter oscillatory behaviors Sørensen et al. (2016).

5.3. Measured Servo Motor Speeds

Figure 17 presents the measured speeds of M_1 and M_2. In motion mode, the speed of M_2 is around 2.08 (k_{speed}) times the speed of M_1, and they have the same rotational direction. In load-holding mode, these two speeds settle to zero when p_{pb} reaches 4 bar. The system turns from load-holding to motion mode at transition points A and C. The pressure level control loop rapidly increases (positive direction) the speed (ω_2) of M_2 to increase the pressure p_{pa} to p_a. The system pressure control loop decreases (negative direction) the speed (ω_1) of M_1 to increase the minimum pressure (p_{pb}) over 10 bar to activate the load-holding valves. In this case, the pressure p_{pa} must be increased much faster than p_{pb} to prevent SV oscillating. Therefore, ω_2 has a much higher peak value than ω_1 at points A and C. The system turns from motion to load-holding mode at transition points B and D. The load-holding control loop commands two servo motors to decrease the pressure (p_{pb}) to deactivate the load-holding valves. ω_2 is two times and opposite direction of ω_1.
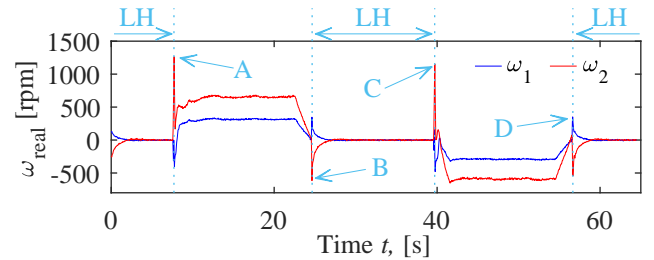
Figure 17: Measured Servo motor speeds.

5.4. 2M2P MCC Energy Efficiency

The 2M2P MCC system power transfer and energy efficiency are addressed in this section. When the piston extends, the system works in pumping mode (quadrant I). When the piston retracts, the system works in motoring mode (quadrant IV). The total servo motor shaft power (P_M) and the cylinder output power (P_C) are presented in Figure 18. P_M is calculated via Equations 39, 40, and 41.

$$P_{M1} = T_1 \cdot \omega_1 \qquad (39)$$

$$P_{M2} = T_2 \cdot \omega_2 \tag{40}$$

$$P_{\mathrm{M}} = P_{M1} + P_{M2} \tag{41}$$

T_1 and T_2 are the measured shaft torques of M_1 and M_2. P_{M1} and P_{M2} are the calculated M_1 and M_2 shaft powers. P_{C} is calculated by the measured bore-side pressure (p_{a}) and rod-side pressure (p_{b}) via Equation 20. Figure 18 illustrates that the power differences ($|P_{\mathrm{C}} - P_{\mathrm{M}}|$) in both pumping and motoring modes are of comparable magnitudes. This observation suggests that the power losses in both modes are similar.
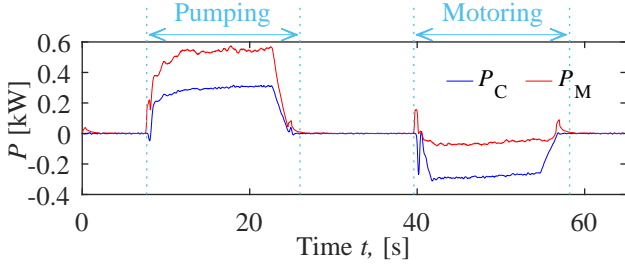
Figure 18: Servo motor and cylinder powers.

The energy efficiency is calculated via $\eta = P_{\mathrm{C}}/P_{\mathrm{M}}$ in pumping mode, and via $\eta = P_{\mathrm{M}}/P_{\mathrm{C}}$ in motoring mode. It should be noted that the cylinder friction is not included in the P_{C} calculation because friction is not directly measurable in the experimental test. Furthermore, servo motor efficiencies are not included in the P_{M} calculation. Therefore, η represents the hydraulic power transfer efficiency in the 2M2P MCC. A moving average filter is used on η to remove noise. The filtered η is presented in Figure 19. η is approximately 56 % in pumping mode, much higher than the conventional valve-controlled hydraulic circuits used in a similar crane system Hagen et al. (2019).

η is approximately 24 % in motoring mode, representing the hydraulic power transfer efficiency in energy regeneration. As mentioned earlier, the power losses in both pumping and motoring modes are comparable. Moreover, the powers exerted by the cylinder in both modes are equal. Consequently, the regenerative efficiency is significantly lower than the efficiency observed in pumping mode. In theory, the regenerated energy can be fed to the grid or a battery. However, the regenerated energy is dissipated by an electric resistor because of lacking required facilities. It
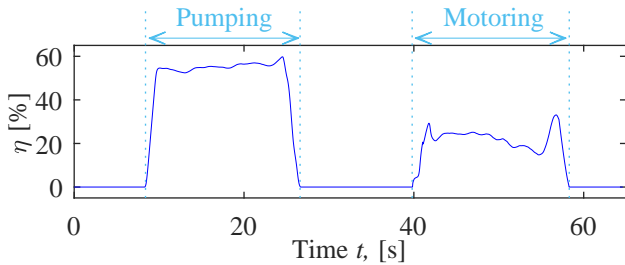
Figure 19: Hydraulic power transfer efficiency.

is important to note that, as shown in Figure 20, the M_2

outputs and regenerates more power than M_1 in pumping and motoring modes. Therefore, M_2 and P_2 should have higher rated powers than M_1 and P_1 to maximize the 2M2P MCC's overall output power limit. However, this factor was not revealed when designing the test facility. The M_2 rated power (1.7 kW) is much lower than the M_1 rated power (2.7 kW). Therefore, the overall output power of the 2M2P MCC testbench is limited.
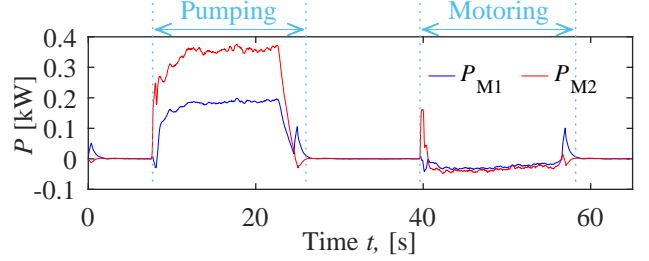
Figure 20: Servo motor shaft powers.

6. Discussion

Based on the data presented in Figure 20, it shows that the power output of the M_2 shaft is significantly greater than that of the M_1 shaft in pumping mode. This can be attributed to the higher flow rate and the greater pressure increment across P_2 compared to P_1. The higher flow rate across P_2 is due to the area ratio of the rod area to the annular area (A_r/A_b), which is 1.04. Additionally, the greater pressure increment across P_2 results from the system pressure control loop controlling the rod-side pressure, the low-pressure side of P_1, to the reference pressure. In contrast, the low-pressure side of P_2 is connected to the accumulator (3 bar). Therefore, as the control reference pressure increases, the power ratio (P_2/P_1) of the M_2 shaft power over the M_1 shaft power also increases in pumping mode. This finding is further supported by the validated simulation model, as depicted in Fig. 21. When the control reference pressure increases from 10 to 40 bar, the power ratio increases from 1.44 to 3.20. Because the load-holding valve activating pressure is 10 bar, the M_2 rated power needs to be at least 1.44 times higher than the M_1 rated power in the proposed 2M2P MCC.
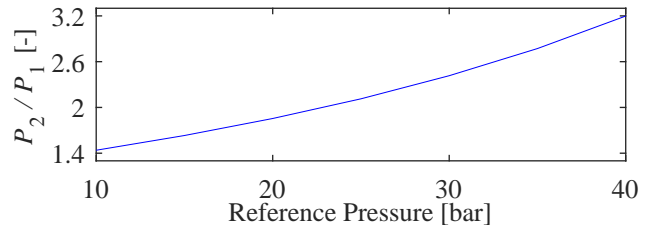
Figure 21: Ratio of servo motor shaft powers.

However, M_2 and P_2 can only contribute to the cylinder output power in quadrant I or cylinder power regenera-

tion in quadrant IV. In quadrant II, the cylinder regenerated power comes solely from M_1 and P_1, while M_2 and P_2 compensate for the cylinder differential flow and control the minimum cylinder pressure (p_{pa}). In quadrant III, the cylinder output power comes solely from M_1 and P_1. Although M_2 and P_2 can regenerate a small amount of cylinder power when compensating for the cylinder differential flow and controlling the minimum cylinder pressure (p_{pa}), they cannot contribute to the cylinder output power in quadrants II and III. Therefore, the proposed 2M2P MCC is more suitable for applications that operate only in quadrants I and IV, such as the crane used in this paper, than for applications that operate in all four quadrants, such as the knuckle boom cylinder circuit on offshore cranes Zhao et al. (2022). Application of the proposed 2M2P MCC in the knuckle boom cylinder circuit on offshore cranes results in greater energy losses than the 1M1P counterpart when the drive unit is mounted on the knuckle boom cylinder. This is due to the larger mass of the 2M2P MCC drive unit, even at the same output power level as the 1M1P MCC, provided that M_2 and P_2 offer higher output power than M_1 and P_1 Zhao and Bhola (2023).

7. Conclusions and Future Work

7.1. Conclusions

A 2M2P MCC can achieve precise control over the piston position and the minimum cylinder pressure. However, its status as a MIMO system presents significant challenges in MIMO control algorithm analysis and design. Moreover, implementing a passive load-holding function further complicates the matter. These challenges make it difficult to apply a 2M2P MCC to real-world applications. This paper proposes a novel motor-controlled cylinder and a control algorithm to overcoming these challenges through the following key aspects:

- A novel two-motor-two-pump motor-controlled cylinder with passive load-holding function was implemented on a laboratory crane system.

- A dynamic model of the system was developed and experimentally validated, providing a valuable simulation tool for future analysis and control design.

- A control algorithm that consists of four control loops to achieve precise control over the piston position and minimum cylinder chamber pressure, as well as a smooth transition between motion and load-holding modes was designed.

- The position tracking error falls within -3.2 mm to 2.3 mm, and the average value is 0.39 mm. The minimum cylinder pressure (p_b) is well controlled above 25 bar.

- The overall system energy efficiency is about 56 % in pumping mode and 24 % in energy regeneration mode.

- Upon analysis, it is found that the output powers of the main electric servo motor and hydraulic pump exceed those of the main electric servo motor and hydraulic pump. Therefore, 2M2P MCCs are more suit-

able for applications that operate in quadrants I and IV.

In conclusion, the experimental results presented in this paper verify the efficacy of the proposed control algorithm and the functionality of the 2M2P MCC. This technique has the potential to be extended to a wide range of industrial applications, particularly those that require a smooth transition between motion and load-holding modes, such as industrial cranes and pitch angle control systems on wind turbines. Overall, the 2M2P MCC represents a promising approach for improving control and energy efficiency in linear hydraulic systems.

7.2. Future Work

The control algorithm presented in this paper is designed for four-quadrant operations. However, due to limitations of the test facility, only two-quadrant operation was experimentally verified. Furthermore, the load on the system is small; therefore, the cylinder working pressure is low. Hence, the efficiency results can be more convincing if pumps operate at higher pressures. Future work will involve implementing the proposed system and control algorithm in an application that operates in four quadrants, such as the knuckle boom cylinder circuit of a knuckle boom crane. This will enable a more comprehensive evaluation of the system's performance and energy efficiency and further demonstrate its potential for industrial applications.

Furthermore, the potential for even greater system energy efficiency is present, as the regenerated energy in the experiments was not able to be reused due to the limitations of the test facility. If this energy could be effectively stored and reused in subsequent operation cycles, the overall energy efficiency of the system could be further improved. Thus, future work will include a simulation study that investigates the impact of stored and reused regenerated energy on the overall energy efficiency of the system.

Finally, as shown in Figure 17, there are motor speed jerks during the transition from load-holding to motion mode due to the pressure level control loop. These jerks harm the rotating components when the drive is at high power levels. Therefore, future work should cover a control algorithm improvement to remove these jerks.

Acknowledgments

References

Agostini, T., De Negri, V., Minav, T., and Pietola, M. Effect of energy recovery on efficiency in electro-hydrostatic closed system for differential actuator. In *Actuators*, 1. MDPI, page 12, 2020.

Fresia, P., Rundo, M., Padovani, D., and Altare, G. Combined speed control and centralized power supply for hybrid energy-efficient mobile hydraulics. *Automation in Construction*, 2022. 140:104337.

Hagen, D. and Padovani, D. A method for smoothly disengaging the load-holding valves of energy-efficient electro-hydraulic systems. In *Proceedings of the First International Electronic Conference on Actuator Technology: Materials, Devices and Applications*. Online, 2020.

Hagen, D., Padovani, D., and Choux, M. A comparison study of a novel self-contained electro-hydraulic cylinder versus a conventional valve-controlled actuator-part 2: Energy efficiency. *Actuators*, 2019. 8. doi:10.3390/ACT8040078.

Hagen, D., Padovani, D., and Choux, M. Guidelines to select between self-contained electro-hydraulic and electro-mechanical cylinders. In *2020 15th IEEE Conference on Industrial Electronics and Applications (ICIEA)*. IEEE, pages 547–554, 2020.

Hagen, D., Padovani, D., and Ebbesen, M. K. Study of a self-contained electro-hydraulic cylinder drive. In *2018 Global Fluid Power Society PhD Symposium (GFPS)*. IEEE, pages 1–7, 2018.

Hansen, A. H. *Fluid Power Systems – A Lecture Note in Modelling, Analysis and Control*. Springer Nature Switzerland AG, 2023.

Imam, A., Rafiq, M., Jalayeri, E., and Sepehri, N. Design, implementation and evaluation of a pump-controlled circuit for single rod actuators. *Actuators*, 2017. 6:10–16. doi:10.3390/act6010010.

Jalayeri, E., Imam, A., Tomas, Z., and Sepehri, N. A throttle-less single-rod hydraulic cylinder positioning system: Design and experimental evaluation. *Advances in Mechanical Engineering*, 2015. 7(5):1687814015583249.

Jensen, K. J., Ebbesen, M. K., and Hansen, M. R. Novel concept for electro-hydrostatic actuators for motion control of hydraulic manipulators. *Energies*, 2021. 14. doi:10.3390/en14206566.

Ketelsen, S., Andersen, T. O., Ebbesen, M. K., and Schmidt, L. A self-contained cylinder drive with indirectly controlled hydraulic lock. *Modeling, Identification and Control: A Norwegian Research Bulletin*, 2020. 41:185–205. doi:10.4173/mic.2020.3.4.

Ketelsen, S., Schmidt, L., Donkov, V. H., and Andersen, T. O. Energy saving potential in knuckle boom cranes using a novel pump controlled cylinder drive. *Modeling, Identification and Control (Online)*, 2018. 39(2):73–89.

Kjelland, M. and Hansen, M. Offshore wind payload transfer using flexible mobile crane. *Modeling, Identification and Control*, 2015. 36:1–9. doi:10.4173/mic.2015.1.1.

Padovani, D., Ketelsen, S., Hagen, D., and Schmidt, L. A self-contained electro-hydraulic cylinder with passive load-holding capability. *Energies*, 2019. 12. doi:10.3390/en12020292.

Parker, H. Electro-hydraulic actuators for high power density applications. [EB/OL], Accessed July 07, 2023. https://www.parker.com/content/dam/Parker-com/Literature/Hydraulic-Pump-Division/Oildyne-EHA/Compact-EHA-Catalog-HY22-3101E-7-13.pdf.

Qu, S., Fassbender, D., Vacca, A., and Busquets, E. A high-efficient solution for electro-hydraulic actuators with energy regeneration capability. *Energy*, 2020. page 119291. URL https://doi.org/10.1016/j.energy.2020.119291, doi:10.1016/j.energy.2020.119291.

Quan, Z., Quan, L., and Zhang, J. Review of energy efficient direct pump controlled cylinder electro-hydraulic technology. *Renewable and Sustainable Energy Reviews*, 2014. 35:336–346.

Schmidt, L., Ketelsen, S., Brask, M. H., and Mortensen, K. A. A class of energy efficient self-contained electro-hydraulic drives with self-locking capability. *Energies*, 2019. 12(10):1866.

Sweeney T., A. D., Kubinski P.T. Electro-hydraulic actuator mounting. U.S. Patent 8161742 B2, 2012.

Sørensen, J. K., Hansen, M. R., and Ebbesen, M. K. Numerical and experimental study of a novel concept for hydraulically controlled negative loads. *Modeling, Identification and Control*, 2016. 37:195–211. doi:10.4173/mic.2016.4.1.

Zhang, S., Minav, T., and Pietola, M. Decentralized hydraulics for micro excavator. In *Proceedings of 15th Scandinavian International Conference on Fluid Power*. Linköping, Sweden, pages 187–195, 2017.

Zhao, W. and Bhola, M. Comparing compact and remote deployments of a speed-controlled cylinder drive unit on an offshore knuckle boom crane. In *Proceedings of the 18th Scandinavian International Conference on Fluid Power (accepted)*. Tampere, Finland, 2023.

Zhao, W., Ebbesen, M. K., and Andersen, T. O. Identifying the future research trend for using speed-controlled hydraulic cylinders in offshore applications through literature survey. In *Proceedings of 2022 IEEE Global Fluid Power Society PhD Symposium (presented)*. Naples, Italy, 2022.

Zimmerman, J. D., Pelosi, M., Williamson, C. A., and Ivantysynova, M. Energy consumption of an ls excavator hydraulic system. In *Proceedings of ASME 2007 International Mechanical Engineering Congress and Exposition*. Seattle, Washington, USA, pages 117–126, 2007.

A. Crane Modeling

The MATLAB/Simulink model for the laboratory crane system is presented in this appendix. The crane MATLAB/Simulink model, shown in Figure 22, is responsible for handling the kinematic calculations. It takes the hydraulic cylinder force signal from the hydraulic system model and feeds the piston position and velocity signals back to the hydraulic system model.
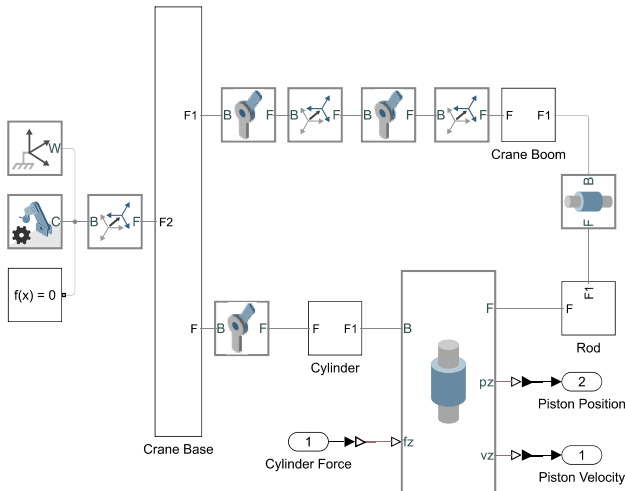
Figure 22: Crane model in Simulink.
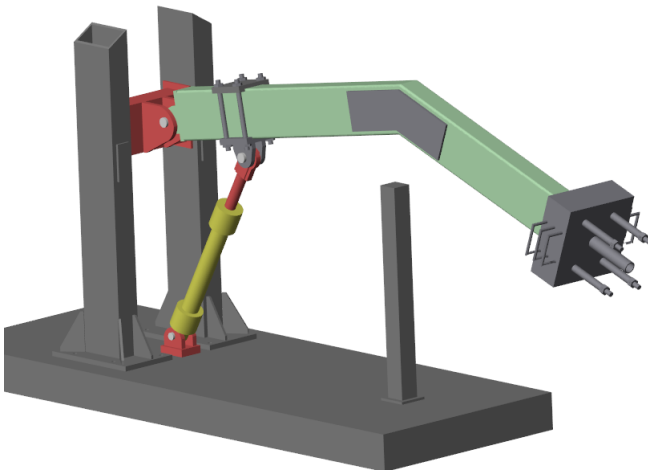
Figure 23: Crane visualization model.

The visualization model of the single-boom crane in Simulink is presented in Figure 23. The model shows the simulated motion of the crane, providing a useful tool for debugging both the hydraulic system model and the control algorithm.

B. Major Components in 2M2P MCC

Table 1 lists the major components used in the 2M2P MCC test facility along with their respective parameters obtained from datasheets provided by the manufacturers.

Table 1: Major Components in 2M2P MCC

Component (Manufacturer)	Specifications
Servo-Motor (M_1) (Bosch Rexroth)	$T_{max} = 16.3$ Nm $N_{max} = 2000$ rpm
Servo-Motor (M_2) (Bosch Rexroth)	$T_{max} = 7.2$ Nm $N_{max} = 2990$ rpm
Axial Piston Pump$_1$ (Bosch Rexroth)	$D_p = 6$ cc/rev.
Axial Piston Pump$_2$ (Bosch Rexroth)	$D_p = 3$ cc/rev.
Shuttle valve (Bucher Hydraulics)	$p_{max} = 350$ bar $Q_{max} = 16$ L/min
Load Holding Valve (Sun Hydraulics)	$p_{max} = 345$ bar $Q_{max} = 227$ L/min $p_{pilot} = 10$ bar
Check Valve (Bosch Rexroth)	$p_{max} = 420$ bar $Q_{max} = 120$ L/min $p_{crack} = 0.2$ bar
Pressure Relief Valve (Bosch Rexroth)	$Q_{max} = 50$ L/min $p_{max} = 400$ bar
Hydraulic Cylinder (LJM Hydraulik)	$D = 65$ mm $d = 43$ mm $L = 400$ mm
PLC (Bosch Rexroth)	RAM 512 MB SERCOS